Ceramics International 48 (2022) 9107–9113

Contents lists available at ScienceDirect

Ceramics International

journal homepage: www.elsevier.com/locate/ceramint

Additive manufacturing of Ca–Mg silicate scaffolds supported by flame-synthesized glass microspheres

J. Kraxner [a,*], H. Elsayed [b,c], A. Dasan [a], M. Hujová [a], M. Michálková [d], M. Michálek [a], E. Bernardo [b], D. Galusek [a,d]

[a] FunGlass, Alexander Dubček University of Trenčín, Trenčín, Slovakia
[b] Department of Industrial Engineering, Università Degli Studi di Padova, Padova, Italy
[c] Refractories, Ceramics and Building Materials Department, National Research Centre, El-Bohous Str., 12622, Cairo, Egypt
[d] Joint Glass Centre of the IIC SAS, TnUAD, and FChFT STU, FunGlass, Alexander Dubček University of Trenčín, Trenčín, Slovakia

ARTICLE INFO

Keywords:
Ca-Mg silicates
Flame spheroidisation
Solid bioactive glass microspheres
Additive manufacturing technology-DLP

ABSTRACT

Novel manufacturing techniques such as additive manufacturing also referred to as 3D printing hold a critical role in the preparation of novel bioactive three-dimensional glass-ceramic scaffolds. The present paper focuses on the use of Ca–Mg silicates microspheres ($Ca_2MgSi_2O_7$, i.e. 40 mol% CaO, 20% MgO and 40% SiO_2) for the fabrication of 3D structures by additive manufacturing. In the first step, the crystallization of the åkermanite system was avoided, by feeding nearly fully crystallized precursor powders prepared by conventional melt quenching into oxygen-methane (O_2/CH_4) torch, and solid glass microspheres (SGMs) with diameters bellow 63 μm were prepared. In the second step, the crystallization was utilized to control the viscous flow of SGMs during firing of reticulated scaffolds, obtained by digital light processing (DLP) of the SGMs suspended in a photocurable acrylate binder. The spheroidal shape facilitated a high solid content, up to 77 wt% of the SGMs in the suspension. After burn-out of the organic binder, a fast sintering treatment at 950 °C, for 30 min, led to scaffolds preserving the macro-porosity from 3D printing model (diamond cell lattice) but with well densified struts. The crystallization of 3D scaffolds during the sintering process led to 3D structures with adequate strength-to-density ratio.

1. Introduction

Glasses have been long investigated for their use in the repair, restoration, and regeneration of tissues within the human body. In particular, Hench revolutionized the use of glassy materials for biomedical applications since the discovery of phospho-silicate Bioglass® (known as 45S5), during the late 1960s; subsequent studies have demonstrated the suitability of many other glass systems, silicate-based, phosphate-based or even borate-based [1,2]. In many cases, the controlled crystallization of glasses has been proposed as a way to increase strength and toughness, leading to a vast range of bioactive glass-ceramics, including but not limited to well-established Cerabone® [3] and Biosilicate® [4]. Parallel activities were focused on polycrystalline ceramics, among which Ca–Mg silicates, such as åkermanite, ($Ca_2MgSi_2O_7$ or $2CaO{\cdot}MgO{\cdot}2SiO_2$) and diopside ($CaMgSi_2O_6$, or $CaO{\cdot}MgO{\cdot}2SiO_2$), are receiving a growing interest [5,6]. Compared to wollastonite ($CaSiO_3$), studied in polycrystalline ceramic or as major crystal phase in bioactive glass-ceramics, Ca–Mg silicates are generally stronger and are subjected to a slower degradation in body fluids; in addition, the ionic products may stimulate cell proliferation [7–9].

Some interesting silicates may be prepared either by a 'ceramic route' (sintering of crystalline powders, e.g. obtained by solid state reactions) or a 'glass route' (i.e. crystallization of a precursor glass). In the specific field of Ca–Mg silicates, this opportunity has been demonstrated for binary systems, i.e. based on the coupling of wollastonite and diopside (particularly for the composition corresponding to the eutectic between the two phases [10,11]). To the authors' knowledge the glass route has not been explored yet for a glass with åkermanite stoichiometry, for the intrinsically high crystallization tendency of the melt [12].

The present paper aims at presenting a new glass-based route to Ca–Mg silicate ceramics, using glass microbeads of the corresponding composition. Spherical microparticles have been already proposed for delivery of glass and glass-ceramic biomaterials into the body in particulate form: the rounded shape may be favourable for bone defect

* Corresponding author.
E-mail address: jozef.kraxner@tnuni.sk (J. Kraxner).

https://doi.org/10.1016/j.ceramint.2021.12.095
Received 8 September 2021; Received in revised form 18 November 2021; Accepted 8 December 2021
Available online 13 December 2021

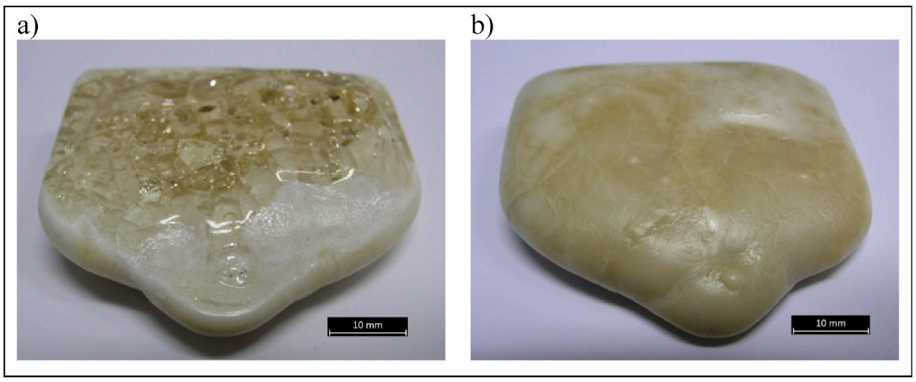

Fig. 1. Glass-ceramic precursors prepared by melt-quenching process on the stainless steel, (a – top and b – bottom side).

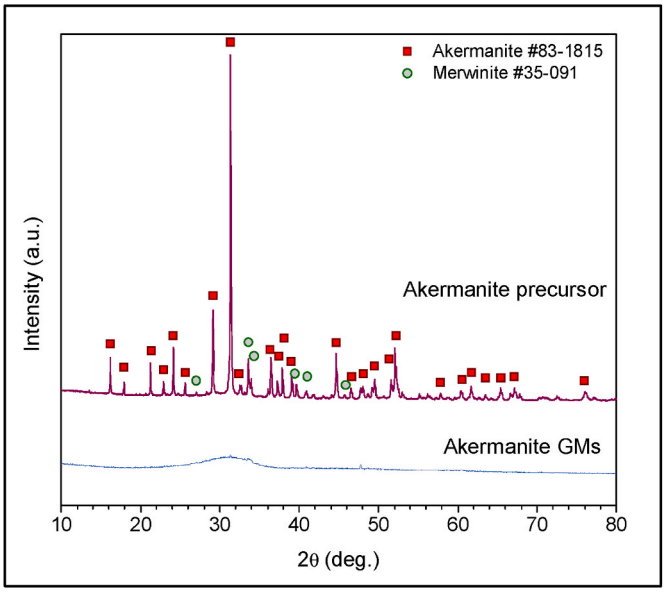

Fig. 2. Diffraction patterns of the precursor powder prepared by melt quenching and of the glass microbeads.

Table 1
Comparison of the theoretical composition, in wt.%, of the åkermanite ($Ca_2MgSi_2O_7$) with the experimental, semi quantitative values obtained by SEM-EDS analysis, before, and after flame synthesis.

Oxide	CaO	MgO	SiO_2
Åkermanite (theoretical composition)	41.14	14.78	44.08
Åkermanite precursor (prepared by melting process)	41.9 ± 0.6	14.8 ± 0.4	43.4 ± 0.5
Åkermanite solid glass microspheres (prepared by flame synthesis)	42.7 ± 0.6	14.0 ± 0.4	43.3 ± 0.5

filling applications, due to denser packing and predictable flow characteristics during injection, compared to irregularly shaped microparticles [13]. In some cases, the microbeads can be engineered to be porous or hollow, allowing encapsulation of other biomedically relevant components [14,15].

For biomaterials and beyond, microspheres are particularly interesting also for additive manufacturing: the reduced friction, together with round particles of controlled size, are advantageous for creating thin powder beds with high flowability [16]. Very recent investigations have specifically dealt with microbeads as precursors for selective laser sintering of complex glass architectures [17,18]. Currently, 3D printing technologies, such as fused deposition modeling (FDM), SLA, selective laser sintering/melting (SLS/SLM), and digital light processing (DLP), have been widely used in various fields including industrial design, sculpture, clothing, automotive, construction, and aerospace. The mainstream materials for 3D printing are metals, resins, plastics, and ceramics. While 3D printing of glass materials has been demonstrated on a laboratory-scale [19–21], large-scale commercial application remains elusive in the near future. Excellent properties of glass (optical properties, mechanical properties, thermal stability, and electrical/thermal insulation), make glass an important material, which is widely used in various fields such as chemistry, biology, and optics [22].

Several methods of fabrication of spherical glass particles have been proposed, such as casting of crushed glass particles in a vertical tube furnace [23], pouring of molten glass onto stainless steel plates (to create droplets) [24], sol–gel synthesis and spray drying of sols [25] and flame spheroidisation [26]. The latter consists of the feeding of a torch ('flame synthesis' apparatus) with various solid precursors; the process is relatively fast and inexpensive, with great flexibility in terms of chemical composition of the prepared microbeads. A key criterion for obtaining uniform spheres without agglomeration is the particle separation before entering the flame. The residence time in the flame is also an important factor, as larger particles require a longer time to be melted. Several studies reported the development of high temperature flame techniques, utilising propane/oxygen, acetylene/oxygen, petrol/oxygen or natural gas/air reactions [27–30]. Torches based on CH_4/O_2 have been recently applied to prepare: i) spherical particles in different forms e.g. solid, hollow and porous [31,32]; ii) glass microspheres with different chemical composition and melting temperature up to 2200 °C [33]; iii) fully amorphous microbeads also from the systems with high crystallization rates [34,35].

The present study aims at introducing several novelties: a) successful preparation of glass microspheres from crystalline precursor in åkermanite stoichiometry with high crystallization rate by application of flame synthesis technique; b) spherical åkermanite glass microparticles below 50 μm enables to use of a high solid loading in the suspension (77 wt%) for their higher packing density achieved by spherical shape when compared with irregular particles; c) in comparison with the literature [36] on åkermanite bioceramics viscous flow sintering implies lower firing temperatures and times.

2. Experimental procedure

A melt corresponding to åkermanite stoichiometry ($CaO/MgO/SiO_2$ = 40/20/40 mol.%) was prepared by heating a mixture of analytical grade purity (≥99%) raw materials (SiO_2 and $CaCO_3$: Centralchem, Bratislava, Slovakia; MgO: Sigma-Aldrich, Bratislava, Slovakia), in a Pt10% Rh crucible. The batch was heated for 2 h, in ambient atmosphere in a Superkanthal furnace, at the maximum temperature of 1530 °C. The homogeneity was ensured by repeated hand mixing of the melt. To determine the influence of quenching and to favour the glass formation,

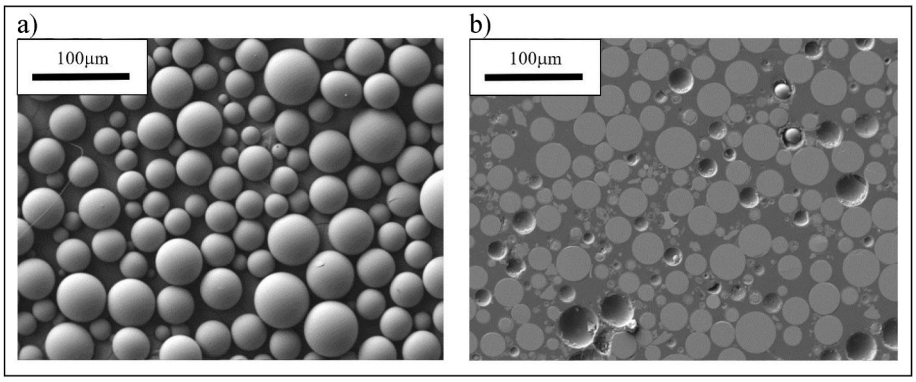

Fig. 3. SEM micrographs of solid glass microspheres prepared by flame synthesis (a) and their cross sections (b).

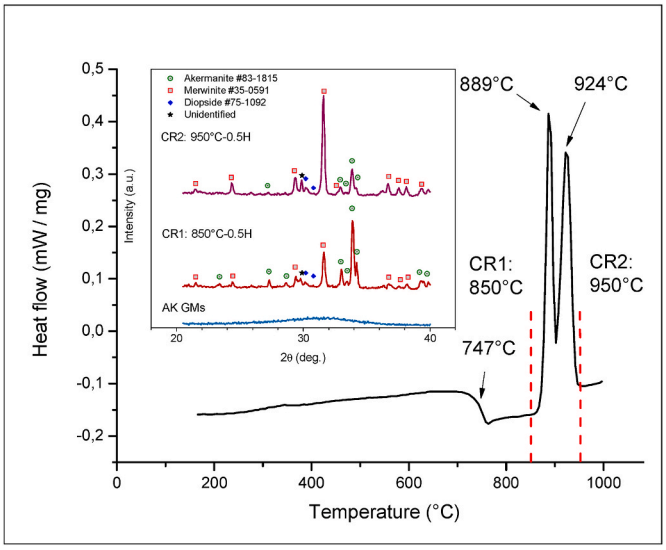

Fig. 4. DSC plot of prepared glass microsphere and XRD patterns of glass microspheres studied after preparation and after firing at 850 °C (CR1) and 950 °C (CR2).

one part of the melt was poured onto a stainless-steel plate, whereas the second part was poured into deionized water (quenched). The quenched glass was crushed, sieved through a 63 µm analytical sieve and used as the precursor for preparation of glass microbeads.

The precursor was fed into an oxygen-methane (O_2/CH_4) torch ('flame synthesis' apparatus) with a vacuum powder feeder, at a rate of 2.5 g/min, using oxygen carrier gas. Spherical molten particles were formed in high temperature oxy-methane flame (estimated temperature 2200 °C) and then quenched by spraying in distilled water, to form solid glass microspheres (SGMs). The SGMs were separated from distilled water by filtering through a ceramic filter with the pore size <0.3 µm.

The thermal behaviour of the glass microspheres in the temperature range from 25 to 1000 °C was studied by differential scanning calorimetry (DSC, Netzsch STA 449 F1 Jupiter, Selb, Germany) at a heating rate of 10 °C/min. The crystallization behaviour of the precursor and SGMs was studied by X-ray powder diffraction analysis (XRD; Bruker AXS D8 Advance, Karlsruhe, Germany), on powdered samples. The XRD patterns were analysed using the Match! Program package (Crystal Impact GbR, Bonn, Germany), supported by the data from the PDF-2 database (ICDD-International Centre for Diffraction Data, Newtown Square, PA, USA). Selected patterns were subjected to refinements according to Rietveld's method, by the Panalytical HighScore software package, supported by the PDF4 crystallographic database.

A photocurable mixture was prepared by mixing åkermanite glass microspheres with a commercially available photocurable acrylic polymer (FTD Standard Blend 3D Printing resin, FunToDo, Alkmaar, The Netherlands), already comprising a suitable photoinitiator and photoabsorber, at a solid loading of 77 wt%. The mixture was first homogenized for 10 min at 2000 rpm, using a planetary mixer (Thinky Are 250, Intertronics, Kidlington, UK), and then printed using a DLP machine (3DLPrinter-HD 2.0, Robot Factory S.R.L., Milano, Italy), operating in the visible light range (between 400 and 500 nm). The layer thickness was set to 100 µm, combined with an exposure time of 8 s/layer. After cleaning in an ultrasonic bath with isopropanol for 3 min, the samples were subjected to a secondary curing step, in a UV curing chamber (operating wavelength 365 nm, Robot Factory S.R.L., Mirano, Italy), for 15 min. DLP-3D printed 'green' samples with dimensions 12 × 12 × 12 mm were debinded at 650 °C for 5 h, at a heating rate of 0.1 °C/min.

Binder-free samples were subsequently sintered at T > 850 °C; optimized samples were densified operating with a fast-heating rate (all samples directly put in the furnace at the selected firing temperature), at 950 °C, for 30 min (followed by natural cooling). The geometrical density was calculated as the mass/volume ratio of regular samples (mass determined by an analytical balance; dimensions measured with a digital calliper). The apparent and true density values were measured on bulk samples (scaffold) and powders by He gas pycnometer (Micromeritics AccuPyc 1330, Norcross, GA, USA). Open, closed, and total porosities were computed according to the measured density values. The compressive strength of the scaffolds was measured at room temperature trough a Universal Testing Machine (Galdabini 1890, Cardano al Campo, VA, Italy) operating at a crosshead speed of 0.5 mm/min. Each data point of the mechanical and physical properties represents the average value of at least 10 individual measurements.

The morphology and chemical composition of prepared precursor powders, microspheres, and printed 3D åkermanite scaffolds were investigated by optical stereomicroscopy (AxioCamERc 5 s Microscope Camera, Carl Zeiss Microscopy, Thornwood, NY, USA), and scanning electron microscopy (SEM, FEI Quanta 200 ESEM, Eindhoven, The Netherlands, and Jeol JFM 7600, Tokyo, Japan - equipped with energy dispersive spectroscopy module, EDS, Oxford, UK), respectively.

3. Results and discussion

A simple demonstration of a high crystallization rate of the melt with åkermanite composition is shown in Fig. 1. When cast on a cold stainless steel plate, only the part of the melt in direct contact with the plate (bottom part) remained glassy (Fig. 1a). The upper part, experiencing a slightly slower cooling, was completely crystallized (Fig. 1b) which was confirmed by XRD (Fig. 2-Akermanite precursor). Cracks were created during the quenching process in areas where melt was in contact with a metal plate (Fig. 1a) which is caused by different cooling rates as well as due to the different coefficients of thermal expansion between the glass and ceramic Fig. 1b. Even though the quenched glass/glass-ceramic

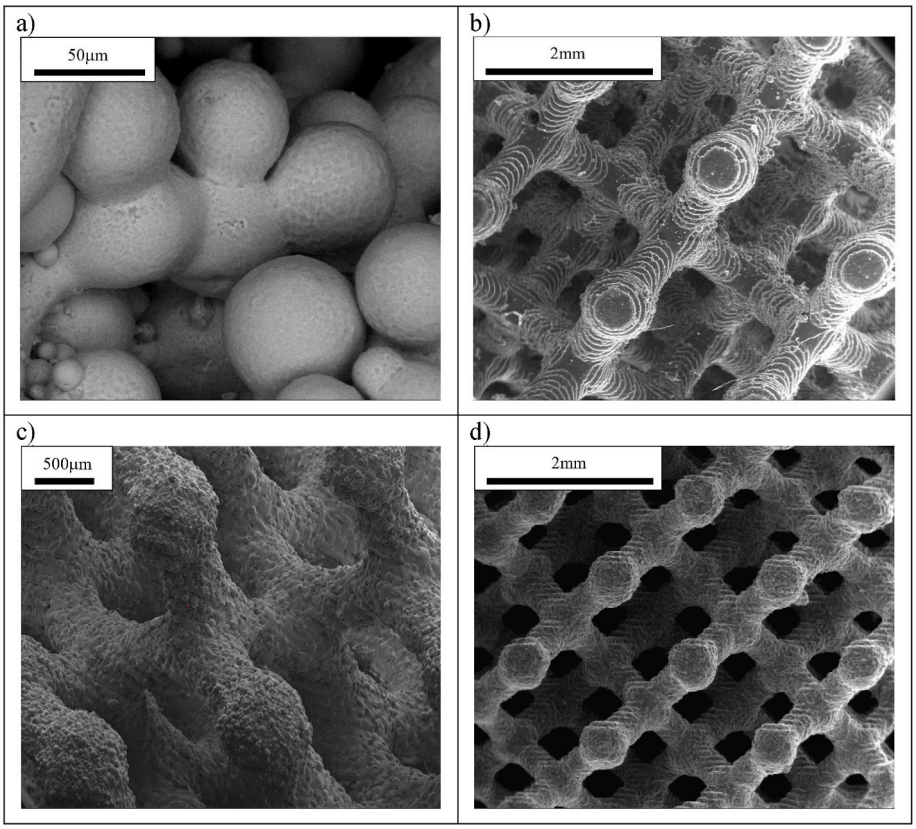

Fig. 5. Microstructural details: a) sintering test on unbound particles (950 °C, 30 min); b) resin/microbeads scaffold; c,d) fast fired scaffold (950 °C, 30 min).

Table 2
Density and strength determinations.

Property	Value
Geometrical density, ρ_{geom} (g/cm^3)	0.54 ± 0.03
Apparent density, ρ_{app} (g/cm^3)	3.01 ± 0.01
True density, ρ_{true} (g/cm^3)	3.02 ± 0.01
Total porosity [P = 100·(1-ρ_{geom}/ρ_{true})] (vol%)	83 ± 1
Open porosity [OP = 100·(1-ρ_{geom}/ρ_{app})] (vol%)	82 ± 1
Closed porosity [CP=P-OP] (vol%)	≈1-2
Compressive strength, (MPa)	1.7 ± 0.2
Bending strength of the solid phase, σ_{bend} (MPa)	~110

contained pores and cracks, the flame synthesis technique provided the complete remelting of fine glass-ceramic particles, previously obtained by the crushing of the 'precursor' shown in Fig. 1.

The mineralogical analysis of crushed crystallized material prepared by quenching on the metal plate is shown in Fig. 2 (top pattern). The diffraction lines matched mostly those of åkermanite ($Ca_2MgSi_2O_7$, i.e. $2CaO{\cdot}MgO{\cdot}2SiO_2$, PDF #83–1815). Diffraction lines unambiguously assigned to another, Ca-richer Ca–Mg silicate merwinite were also identified. Merwinite ($Ca_3MgSi_2O_8$, i.e. $3CaO{\cdot}MgO{\cdot}2SiO_2$, PDF #89–2432) formation was likely due to local overconcentration of Ca^{2+} ions, with the residual glass enriched in MgO and SiO_2 after crystallization of åkermanite. The chemical composition of prepared åkermanite precursor and glass microspheres are reported in Table 1.

Flame synthesis converted highly crystalline precursor powders into fine (<63 μm), uniform glass microspheres, with smooth surfaces, as shown by Fig. 3a. No internal cavity, crack or morphological features suggesting presence of crystals could be distinguished in polished cross-sections, as shown in Fig. 3b (particles embedded in epoxy resin). The

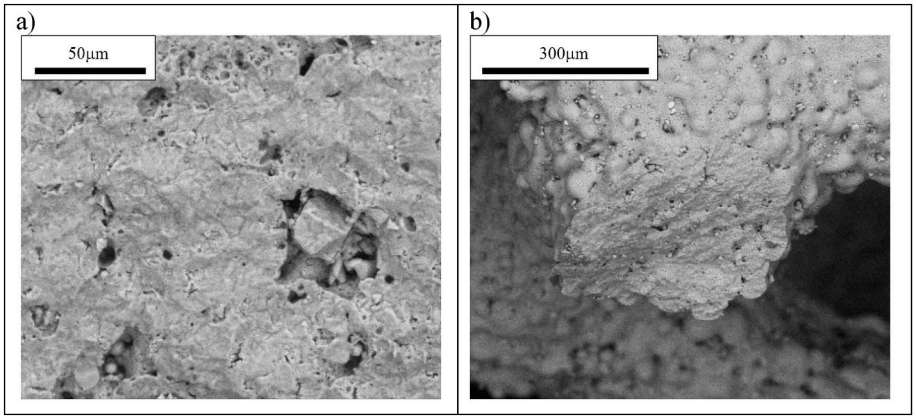

Fig. 6. Details of broken struts: a) internal voids; b) full cross-section.

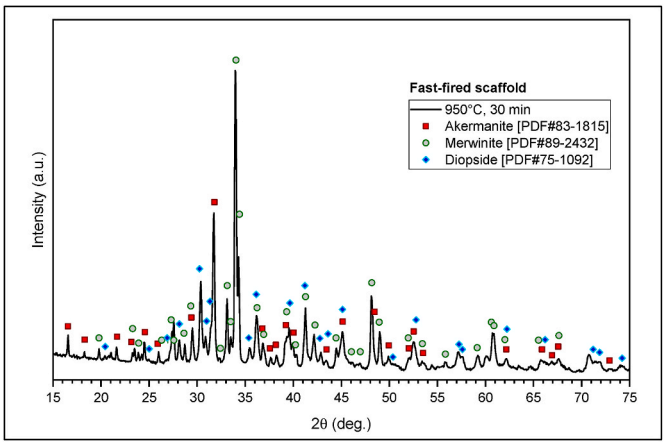

Fig. 7. XRD pattern of fast-fired 3D scaffold at 950 °C.

amorphous nature of the microspheres was confirmed by the mineralogical analysis (Fig. 2, bottom pattern).

The microbeads with the chemical composition deviating only negligibly from åkermanite stoichiometry (Table 1), were further studied by differential scanning calorimetry, to disclose the crystallization behaviour. The DSC plot of the prepared microspheres, shown in Fig. 4, exhibits several well distinguishable endothermic and exothermic effects. In particular, the glass transition temperature (T_g) was evidenced by the endothermic effect at ~750 °C, whereas two strong, partially overlapping exothermic effects, with maxima at ~890 °C and ~925 °C, indicated the formation of two distinct crystal phases.

To clarify the nature of the exothermic effects, isothermal annealing experiments were conducted at 850 °C and 950 °C (30 min) i.e. at the endpoints of the crystallization interval, by direct insertion of loose powders on Pt sheet into a furnace. As illustrated by the inset in Fig. 4, annealing at 850 °C (CR1) led to substantial crystallization of merwinite, while the higher temperature (950 °C = CR2) favoured åkermanite. The XRD analysis revealed also traces of diopside ($CaMgSi_2O_6$, i.e. $CaO{\cdot}MgO{\cdot}2SiO_2$, PDF #75–1092). Moreover, one peak was not identified (Fig. 4).

The two overlapping crystallization phenomena were consistent with findings in the literature [12] concerning the åkermanite–gehlenite system. Åkermanite ($2CaO{\cdot}MgO{\cdot}2SiO_2$) is isomorphic with gehlenite ($2CaO{\cdot}Al_2O_3{\cdot}SiO_2$), and a broad range of solid solutions may be formed. Ca^{2+} ions may be sandwiched between pure Mg-silicate sheets (in pure åkermanite) as well as in sheets in which Mg^{2+}/Si^{4+} ion couples are replaced by 2 Al^{3+} ions, partially (in solid solutions) or completely (in pure gehlenite) [37]. Only melts corresponding to a substantial replacement (Mg^{2+}/Si^{4+} replaced by Al^{3+} ions for more than 60% of their lattice sites) form glasses which devitrify 'homogeneously', i.e. leading directly to a crystal product with the same chemical composition. In other cases, merwinite appears as an intermediate phase, due to a lower activation energy of crystallization (<690 kJ/mol), compared to that of åkermanite (~1000 kJ/mol) [12]. The difference is due to the much simpler crystal structure of merwinite, featuring 'insular' SiO_4 groups surrounded by Ca^{2+} and Mg^{2+} ions [38].

The two crystallization peaks could complicate the perspective of obtaining useable articles from glass microbeads, according to a 'sinter-crystallization' mechanism, i.e. viscous flow sintering with concurrent crystallization [39]. In this framework, it is important to find a trade-off between densification and retention of the shape of the green object. A characteristic temperature interval, consisting of the gap between transition temperature (T_g) and crystallization temperature (T_{cryst}) is typically considered as a reference [40]. T_g marks the passing from glass to liquid state, enabling viscous flow densification, whereas T_{cryst} marks the appearance of rigid inclusions in the mass of softened glass. The abrupt increase of viscosity, due to the formation of these rigid inclusions, is a limiting factor for viscous flow (determining the "freezing" of the shape of the green object, except for a homogeneous shrinkage) [41].

Operating with glasses having a distinct single crystallization peak and featuring a wide gap between glass transition and crystallization temperature (>200 °C), sintering at the exact crystallization temperature generally offers an optimum balance between densification and crystallization. Narrower gaps, like in the present case, may favour the crystallization, so that densification is very limited. Only necking of adjacent particles may be observed, even if a very fast heating at the upper end of the crystallization interval is applied (Fig. 5a).

The use of åkermanite glass microbeads had quite surprising effects on both printing and firing. In a first step, due the lower increase of viscosity offered by round particles in suspension, compared to 'angular' particles, the solid content could be raised up to 77 wt%, obtaining well-defined scaffolds with diamond cell architecture (Fig. 5b). Higher solid loading led to difficulty in printing process. In a second step, such high solid loading maximizing the contact points between particles, was found to prevent the collapse of green scaffolds after debinding at 650 °C (well below T_g, i.e. without the possibility of joining adjacent particles by viscous flow sintering). Finally, direct heating at 950 °C of three-dimensional scaffolds (after debinding) led to a much more substantial densification than in the case of loose particles (Fig. 5c). The diamond cell architecture was preserved (Fig. 5d).

As shown in Table 2, the porosity of fast-fired scaffolds was substantial (P = 0.82 = 82 vol%) and almost completely open, but practically attributable only to the specific design used for printing. In fact, the struts contained only minor pores, as shown in Fig. 6a; the same image also illustrates the mutual joining of particles and the precipitation of crystals. In addition, fracture surfaces, like the one shown in Fig. 6b, contained no evidence of delamination between printed layers. The roughness of the external surfaces can be seen as a promising feature for the application of scaffolds in bone tissue engineering, for cell attachment and infiltration of body fluids.

The substantial crystallization in fast-fired scaffolds was confirmed by the mineralogical analysis, shown in Fig. 7. Quite surprisingly, merwinite appeared as the main phase, as in the case of loose particles sintered at lower temperature; diopside was also well visible. The amount of identified crystalline phases in the different samples (CR1, CR2 and fast fired 3D scaffold at 950 °C) were finally quantified by Rietveld refinements of the XRD patterns. The results are shown in Table 3.

The 3D scaffold sintered under the same conditions as the resin free CR2 sample (sintered at identical temperature, 950 °C) contained a lower amount of åkermanite and a significantly higher amount of diopside phase. One possible cause for this anomaly is the introduction of photocurable acrylic polymer (Standard Blend 3D Printing resin) into the system. The safety data sheet of used resin (see section 3) specifically

Table 3
Summary of sintering conditions and amount of identified crystalline phases.

Sample	Temperature [°C]	Holding time [min]	Identified crystalline phases [wt%]		
			Åkermanite	Merwinite	Diopside
CR1	850	30	46.2	53.8	–
CR2	950	30	87.5	10.9	1.6
3D scaffold	950	30	19.2	54.0	26.8

mentions a phosphine oxide based photo-initiator [42]. Phosphine oxides are phosphorus compounds with the formula OPX_3, where X = alkyl or aryl groups [43]. It cannot be excluded that, upon firing, the photo-initiator decomposes, yielding P_2O_5, which is known to act in glass-ceramics as nucleation agent [44–46].

The formation of diopside was consistent with the glass stoichiometry. In fact, the stoichiometry of åkermanite matches with the mixing of merwinite and diopside (åkermanite = 50 mol% merwinite+50 mol% diopside), as follows:

$$2 \times 2CaO{\cdot}MgO{\cdot}2SiO_2 \leftrightarrow 3CaO{\cdot}MgO{\cdot}2SiO_2 + CaO{\cdot}MgO{\cdot}2SiO_2 \quad (1)$$

To form only åkermanite, different heating conditions or even at post-treatment of scaffolds can be considered. However, the observed 'splitting' of åkermanite glass in diopside and merwinite, instead of homogeneous crystallization into åkermanite, was not considered as an issue, given the biocompatibility and bioactivity of both merwinite and diopside [7].

The observed compressive strength of ~1.7 MPa was considered satisfactory, given the abundant porosity and the possible severe stress concentration around defects. According to the Gibson&Ashby model for highly porous lattices, the crushing strength of the body (σ_{comp}) is a measure of the bending strength of the solid phase positioned in the struts (σ_{bend}), 'downscaled' by an exponential function of relative density (ρ_{rel} = 1-P), as follows:

$$\sigma_{comp} \sim 0.2{\cdot}\sigma_{bend}{\cdot}(\rho_{rel})^{1.5} \quad (2)$$

The experimental data of compressive strength and relative density were well fitted by a bending strength of the solid phase in the order of 110 MPa, in good agreement with the measured bending strength of glass-ceramic systems [47], despite defects.

In conclusion, åkermanite glass microbeads exhibit a great potential for the manufacturing of Ca–Mg silicate scaffolds, from the overlapping of three rapid operations (melt quenching, flame synthesis, sinter-crystallization) and the easiness of application of DLP printing, which suggests industrial scalability. Some efforts will be dedicated in the future to scaffolds with a more complex porosity distribution, e.g., preparation of porous scaffolds with the use of porous microbeads. Alternative compositions (e.g., Al-doped) will be studied to simplify the processing, by promoting a 'direct' devitrification (transformation of glass into a crystal phase with the same stoichiometry).

4. Conclusions

The main findings of this study may be summarized as follows:

- A homogeneous glass with åkermanite ($Ca_2MgSi_2O_7$) composition cannot be prepared by conventional melting; a two-stage process, consisting of fast cooling of the melt and reuse of a powdered partly crystalline material as a precursor for flame synthesis, yielded completely amorphous particles, with regular spherical shape and uniform dimensions (<63 μm);
- The obtained glass microbeads were advantageous in additive manufacturing experiments by DLP. High solid loading (77 wt%) of microbeads suspended in a photocurable acrylic liquid allows fabrication of scaffolds with a diamond cell design. The packing of microspheres, maximizing the contact between adjacent particles, prevented the collapse of printed structures upon debinding;
- The control of the sinter-crystallization (sintering with concurrent devitrification) of glass microbeads was complicated by the overlapping of two crystallization phenomena, with formation of merwinite ($Ca_3MgSi_2O_8$) preceding that of åkermanite;
- The application of direct heating at 950 °C, for 30 min, designed to promote viscous flow densification, effectively led to formation of åkermanite as the main crystalline phase, only in loose particles (resin free). With particles packed in scaffolds, merwinite and diopside crystallized besides åkermanite during the sinter-crystallization. The rapid treatment at 950 °C for 30 min represented a successful trade-off between densification, retention of the shape imparted by 3D-printing and strength-to-density ratio of the final product.

Declaration of competing interest

The authors declare that they have no known competing financial interests or personal relationships that could have appeared to influence the work reported in this paper.

Acknowledgment

This paper is a part of dissemination activities of project FunGlass. This project has received funding from the European Union's Horizon 2020 research and innovation programme under grant agreement No 739566. Authors also gratefully acknowledge the financial support from Slovak Grant Agency of Ministry of Education, Science, Research and Sport, VEGA 1/0456/20.

References

[1] Larry L. Hench, The story of Bioglass®, J. Mater. Sci. Mater. Med. 17 (2006) 967–978, https://doi.org/10.1007/s10856-006-0432-z.
[2] Julian R. Jones, Review of bioactive glass: from Hench to hybrids, Acta Biomater. 9 (2013) 4457–4486, https://doi.org/10.1016/j.actbio.2012.08.023.
[3] T. Kokubo, A/W Glass-Ceramic: Processing and Properties, Advanced Series in Ceramics an Introduction to Bioceramics, 1993, pp. 75–88, https://doi.org/10.1142/9789814317351_0005.
[4] C. Murilo, Crovace et al.: Biosilicate® — a multipurpose, highly bioactive glass-ceramic. In vitro, in vivo and clinical trials, J. Non-Cryst. Solids 432 (2016) 90–110, https://doi.org/10.1016/j.jnoncrysol.2015.03.022.
[5] S. Palakurthy, et al., A novel cost-effective approach to fabricate diopside bioceramics: a promising ceramics for orthopedic applications, Adv. Powder Technol. 32 (2021) 875–884, https://doi.org/10.1016/j.apt.2021.01.038.
[6] S. Punj, et al., In-vitro biological evaluation of diopside bio-ceramic synthesized from sustainable agro-food waste ashes, Silicon (2021), https://doi.org/10.1007/s12633-021-01484-8.
[7] Armina Khajeh Sharafabadi, et al., A novel and economical route for synthesizing akermanite ($Ca_2MgSi_2O_7$) nano-bioceramic, Mater. Sci. Eng. C 71 (2017) 1072–1078, https://doi.org/10.1016/j.msec.2016.11.021.
[8] Wenlong Liu, et al., Akermanite used as an alkaline biodegradable implants for the treatment of osteoporotic bone defect, Bioact. Mater. 1 (2016) 151–159, https://doi.org/10.1016/j.bioactmat.2016.11.004.
[9] S.K. Venkatraman, S. Swamiappan, Review on calcium- and magnesium-based silicates for bone tissue engineering applications, J. Biomed. Mater. Res. 108 (2020) 1546–1562, https://doi.org/10.1002/jbm.a.36925.
[10] M.A. Sainz, et al., Influence of design on bioactivity of novel $CaSiO_3$–$CaMg(SiO_3)_2$ bioceramics: in vitro simulated body fluid test and thermodynamic simulation, Acta Biomater. 6 (2010) 2797–2807, https://doi.org/10.1016/j.actbio.2010.01.003.
[11] H. Elsayed, et al., Comparative analysis of wollastonite-diopside glass-ceramic structures fabricated via stereo-lithography, Adv. Eng. Mater. 21 (6) (2019) 1801160, https://doi.org/10.1002/adem.201801160.
[12] Allu Amarnath Reddy, et al., Sintering and devitrification of glass-powder compacts in the akermanite–gehlenite system, J. Mater. Sci. 48 (2013) 4128–4136, https://doi.org/10.1007/s10853-013-7225-9.
[13] K.M.Z. Hossain, U. Patel, I. Ahmed, Development of microspheres for biomedical applications: a review, Progr. Biomater. 4 (2015) 1–19, https://doi.org/10.1007/s40204-014-0033-8.
[14] Y. Cai, et al., Porous microsphere and its applications, Int. J. Nanomed. 8 (2013) 1111–1120, https://doi.org/10.2147/IJN.S41271.
[15] S. Freiberg, X.X. Zhu, Polymer microspheres for controlled drug release, Int. J. Pharm. 282 (1–2) (2004) 1–18, https://doi.org/10.1016/j.ijpharm.2004.04.013.
[16] Malvern Instruments Limited, Optimizing Metal Powders for Additive Manufacturing-Exploring the Impact of Particle Morphology and Powder Flowability, 2017.
[17] M. Fateri, A. Gebhardt, Selective laser melting of soda-lime glass powder, Int. J. Appl. Ceram. Technol. 12 (1) (2015) 53–61, https://doi.org/10.1111/ijac.12338.
[18] K.C. Datsiou, et al., Additive manufacturing of glass with laser powder bed fusion, J. Am. Ceram. Soc. 102 (8) (2019) 4410–4414, https://doi.org/10.1111/jace.16440.
[19] A. Dasan, et al., Up-cycling of LCD glass by additive manufacturing of porous translucent glass scaffolds, Materials 14 (2021) 5083, https://doi.org/10.3390/ma14175083.
[20] Ch Inamura et al.: High fidelity additive manufacturing of transparent glass structures, Proceedings of the IASS Annual Symposium 2018 Creativity in Structural Design, July 16-20, (20180), MIT, Boston, USA.

[21] D.G. Moore, et al., Three-dimensional printing of multicomponent glasses using phase-separating resins, Nat. Mater. (2020) 212–217, https://doi.org/10.1038/s41563-019-0525-y.
[22] D. Zhang, et al., 3D printing of glass by additive manufacturing techniques: a review, Front. Optoelectron. 14 (3) (2021) 263–277, https://doi.org/10.1007/s12200-020-1009-z.
[23] H. Fu, et al., Effect of process variables on the microstructure of hollow hydroxyapatite microspheres prepared by a glass conversion method, J. Am. Ceram. Soc. 93 (10) (2010) 3116–3123, https://doi.org/10.1111/j.1551-2916.2010.03833.x.
[24] W. Huang, et al., Strength of hollow hydroxyapatite microspheres prepared by a glass conversion process, J. Mater. Sci. Mater. Med. 20 (2009), https://doi.org/10.1007/s10856-008-3554-7. Article number: 123.
[25] M. Todea, et al., XPS analysis of aluminosilicate microspheres bioactivity tested in vitro, Appl. Surf. Sci. 270 (2013) 777–783, https://doi.org/10.1016/j.apsusc.2013.01.178.
[26] K.M.Z. Hossain, et al., Porous calcium phosphate glass microspheres for orthobiologic applications, Acta Biomater. 72 (2018) 396–406, https://doi.org/10.1016/j.actbio.2018.03.040.
[27] J. R Martinelli, et al., Synthesis and characterization of glass–ceramic microspheres for thermotherapy, J. Non-Cryst. Solids 356 (2010) 2683–2688, https://doi.org/10.1016/j.jnoncrysol.2010.05.006.
[28] S.D. Conzone, et al., In vitro and in vivo dissolution behavior of a dysprosium lithium borate glass designed for the radiation synovectomy treatment of rheumatoid arthritis, J. Biomed. Mater. Res. 88A (2002) 531–542, https://doi.org/10.1002/jbm.10047.
[29] N.J. Lakhar, et al., Titanium phosphate glass microspheres for bone tissue engineering, Acta Biomater. 8 (11) (2012) 4181–4190, https://doi.org/10.1016/j.actbio.2012.07.023.
[30] Q. Wang, et al., Preparation of hollow hydroxyapatite microspheres, J. Mater. Sci. Mater. Med. 17 (2006) 641–646, https://doi.org/10.1007/s10856-006-9227-5.
[31] J. Kraxner, et al., Hollow polycrystalline YAG microspheres by flame synthesis, Mater. Lett. (2017), https://doi.org/10.1016/j.matlet.2017.05.108.
[32] J. Kraxner, M. Michalek, et al., Porous bioactive glass microspheres prepared by flame synthesis process, Mater. Lett. 256 (2019) 126625, https://doi.org/10.1016/j.matlet.2019.126625.
[33] M. Majerová, et al., Crystallization kinetics of Ni-doped $Ca_2Al_2SiO_7$ glass microspheres, J. Therm. Anal. Calorim. 142 (5) (2020) 2111–2121, https://doi.org/10.1007/s10973-020-10154-7.
[34] M. Michálková, J. Kraxner, et al., Viscous flow spark plasma sintering of glass microspheres with YAG composition and high tendency to crystallization, J. Eur. Ceram. Soc. 41 (2) (2021) 1537–1542, https://doi.org/10.1016/j.jeurceramsoc.2020.10.015.
[35] A. Rosenflanz, et al., Bulk glasses and ultrahard nanoceramics based on alumina and rare-earth oxides, Nature 430 (2004), https://doi.org/10.1038/nature02729.
[36] A. Liu, et al., Three-dimensional printing akermanite porous scaffolds for load-bearing bone defect repair: an investigation of osteogenic capability and mechanical evolution, J. Biomater. Appl. 31 (5) (2016) 650–660, https://doi.org/10.1177/0885328216664839.
[37] I.P. Swainson, et al., Neutron powder diffraction study of the åkermanite-gehlenite solid solution series, Phys. Chem. Miner. 19 (1992) 185–195, https://doi.org/10.1007/BF00202107.
[38] Jun Ou, et al., Preparation and in vitro bioactivity of novel merwinite ceramic, Biomed. Mater. 3 (8pp) (2008), 015015, https://doi.org/10.1088/1748-6041/3/1/015015.
[39] M.O. Prado, E.D. Zanotto, Glass sintering with concurrent crystallization, C. R. Chimie 5 (2002) 773–786.
[40] M. Michálková, J. Kraxner, et al., Preparation of translucent YAG glass/ceramic at temperatures below 900°C, J. Eur. Ceram. Soc. 40 (7) (2020) 2581–2585, https://doi.org/10.1016/j.jeurceramsoc.2019.11.011.
[41] G.W. Scherer, Sintering with rigid inclusions, J. Am. Cerarn. SOC. 70 (10) (1987) 719–725, https://doi.org/10.1111/j.1151-2916.1987.tb04870.x.
[42] http://www.funtodo.net/docs-info.html.
[43] B. Thomas, Rauchfuss: phosphorus:an outline of its chemistry ,biochemistry and technology ,fifth edition ,studies in inorganic chemistry, J. Am. Chem. Soc. 118 (33) (1996) 7871, https://doi.org/10.1021/ja965522m, 1996.
[44] H.R. Fernandez, et al., The role of P_2O_5, TiO_2 and ZrO_2 as nucleating agents on microstructure and crystallization behaviour of lithium disilicate-based glass, J. Mater. Sci. 48 (2013) 765–773, https://doi.org/10.1007/s10853-012-6793-4.
[45] K. Ariane, et al., Effect of P_2O_5 and Al_2O_3 on crystallization, structure, microstructure and properties of Li_2O–MgO–Al_2O_3–SiO_2–TiO_2–ZrO_2 glass ceramics, Bol. Soc. Esp. Cerám. Vidr. (2020), https://doi.org/10.1016/j.bsecv.2020.08.004.
[46] W. Höland, et al., P_2O_5 as an effective nucleating agent of lithium disilicate glass-ceramics, Phosphorus Res. Bull. 19 (2005) 36–41, https://doi.org/10.3363/prb1992.19.0_36.
[47] H. Elsayed, et al., Suitability of Biosilicate® glass-ceramic powder for additive manufacturing of highly porous scaffolds, Ceram. Int. 47 (6) (2020), https://doi.org/10.1016/j.ceramint.2020.11.179.